Annals of Communications in Mathematics
Volume 9, Number 4 (2026), 2
DOI: 10.62072/acm.2026.09049
ISSN: 2582-0818
https://www.technoskypub.com/journal/acm/

Research article

A class of A-stable two-step multi-derivative hybrid block methods for stiff initial value problems

O. V. Atabo[1]*, E. O. Senewo[1], B. D. Michael[1], I. G. Ezugorie[1], Q. O. Ahman[1], B. C. Agbata[1],

[1]Department of Mathematics and Statistics, Confluence University of Science and Technology, Osara, Kogi State, Nigeria.

*Corresponding Author: O. V. Atabo. Email: ataboov@custech.edu.ng

Received: 04 September 2026; Accepted: 17 October 2026; Published: 05 November 2026

Citation: O. V. Atabo, E. O. Senewo, B. D. Michael, I. G. Ezugorie, Q. O. Ahman, B. C. Agbata, A class of A-stable two-step multi-derivative hybrid block methods for stiff initial value problems. Ann. Commun. Math. 9 **(2026)**, 2. https://doi.org/10.62072/acm.2026.09049

Abstract: The numerical integration of stiff ordinary differential equations is frequently hindered by the classical Dahlquist barrier and severe absolute stability constraints, forcing a reliance on prohibitively small step sizes or computationally expensive extended formulas. To resolve these algorithmic bottlenecks, this study formulates a robust class of A-stable, two-step multi-derivative hybrid block methods for direct integration. Derived via continuous polynomial power series interpolation and dynamic intra-step collocation, these discrete formulas incorporate analytical higher-order derivatives up to the fourth order to guarantee unconditional A-stability across the open left-half complex plane. Theoretical analysis establishes that the schemes are zero-stable, consistent, and globally convergent, uniformly achieving an algebraic order of eight ($p = 8$). The primary novelty lies in allocating a dynamically shifted single off-grid collocation point within a fourth-derivative architecture, successfully bypassing traditional stability limitations while maintaining a rigidly low step number ($k = 2$). Extensive numerical simulations on severe stiff systems, rapid transient modes, and chemical reaction dynamics demonstrate that the proposed integrators suppress stiffness-induced error accumulation, yielding exceptionally tighter precision bounds and significant computational speedups over existing state-of-the-art block techniques.

Mathematics Subject Classification: 65L05, 65L20
Keywords: Multi-derivative methods, Block integration, A-stability, Convergence analysis, Stiff systems.

1 Introduction

Equations of the form given in Eq. (1) arise frequently in diverse scientific domains including biology, physics, and engineering. These mathematical models are generally intractable analytically, necessitating the development of robust and stable numerical integrators [1]. The core problem in numerical initial-value integration is the efficient resolution of highly stiff systems without suffering from severe order reduction or restrictive stability bounds. As articulated by [2], the essential prerequisites for numerical convergence

Copyright © 2026 The Author(s). Licensee Techno Sky Publications.
This article is an open-access article distributed under the terms and conditions of the Creative Commons Attribution (CC BY) license (https://creativecommons.org/licenses/by/4.0/).

are the synthesis of adequate stability with a sufficiently high order of accuracy. However, the simultaneous enforcement of high order and broad stability regions imposes strict theoretical limitations on classical Linear Multi-step Methods (LMMs), particularly the Dahlquist barrier which asserts that the maximum order of an unconditionally stable LMM cannot exceed $p = 2$ [3].

To circumvent these inherent restrictions, two primary strategies have traditionally been employed: the utilization of block backward differentiation formulas (BBDFs) and the incorporation of intra-step (off-grid) collocation points into LMMs. While both paradigms enhance the stability domain and convergence order, intra-step formulations can introduce algorithmic complexities and increase computational overhead. Hybrid block methods, which occasionally rely on predictor–corrector implementations, also risk increased structural complexity. Over recent decades, these limitations have been mitigated by formulating LMMs designed for direct block implementations (see [4–14]).

An ordinary differential equation is classified as stiff when its Jacobian matrix exhibits eigenvalues with large negative real parts, forcing conventional numerical methods to employ prohibitively small step sizes to maintain absolute stability. Consequently, numerous studies have optimized stiff solvers using BBDFs, generalized Adams-type approaches, or modified continuous extended LMMs that preserve accuracy while accommodating stiffness [15–21]. For instance, [23] established a class of continuous extended LMMs achieving A-stability up to a theoretical maximum order of $p = k+3$. Similarly, [24] formulated generalized Cash-type second-derivative extended backward differentiation formulas via boundary-value frameworks.

Recent paradigm shifts have increasingly focused on multi-derivative integration methods to bypass traditional stability limits. [25] proposed a two-point implicit block technique of the seventh-derivative class, constructed over non-uniform collocation points. For the direct approximation of Eq. (1), researchers including [26–28] have derived extensive families of multi-derivative block methods that achieve rapid convergence. More recently, [29,30] analyzed multi-derivative hybrid block architectures customized for integrating stiff systems.

Despite these advances, a significant gap remains in the literature regarding the formulation of high-order multi-derivative block methods that perfectly balance unconditional A-stability with minimal grid point density. Many existing methods either require excessive step numbers or compromise absolute stability.

The motivation for this study is to bridge this gap. Consequently, the primary objective of this paper is to derive, analyze, and computationally validate a robust class of two-step, multi-derivative numerical formulas designed for the direct integration of stiff initial-value problems. The novelty of this approach lies in the strategic deployment of a dynamic single intra-step point within a fourth-derivative framework. The precise placement of this off-grid collocation point effectively bypasses the traditional Dahlquist stability barriers. Although incorporating higher derivatives introduces additional computational overhead during the evaluation phase, our results demonstrate that the resulting gains in stability, accuracy, and convergence rigorously justify this approach for complex stiff systems.

The remainder of this manuscript is organized as follows: Section 2 outlines the rigorous mathematical formulation of the proposed methods. The analysis of foundational numerical properties, including zero-stability and A-stability, is established in Section 3. The numerical implementation strategy is detailed in

Section 4, followed by numerical experiments on benchmark stiff problems in Section 5. Finally, concluding remarks and future directions are presented in Section 7.
Consider the initial-value problem for a first-order differential system:

$$y' = f(x, y(x)), \qquad y(0) = y_0. \tag{1}$$

And the corresponding second-order differential system:

$$y'' = f(x, y(x), y'(x)), \qquad y(0) = y_0, \qquad y'(0) = y'_0, \tag{2}$$

where $f(x, y(x))$ and $f(x, y(x), y'(x))$ are continuous and differentiable over the integration interval $[a, b]$, and are assumed to satisfy the standard Lipschitz conditions for the existence and uniqueness of solutions over this interval.

2 Formulation of the Methods

This section establishes the mathematical derivation of the proposed multi-derivative techniques. Given the initial approximation y_n at x_n, the methods concurrently advance the solution to obtain y_{n+1}, $y_{n+\frac{3}{2}}$, and y_{n+2} over the discretized mesh points x_{n+1}, $x_{n+\frac{3}{2}}$, and x_{n+2}. Throughout the derivation, standard notation is adopted for higher derivatives such that the first, second, third, and fourth derivatives of $y(x)$ with respect to x are strictly denoted as $f(x, y)$, $g(x, y)$, $u(x, y)$, and $v(x, y)$, respectively. The structural framework of the proposed fourth-derivative single intra-step methods is illustrated in the block diagrams below.

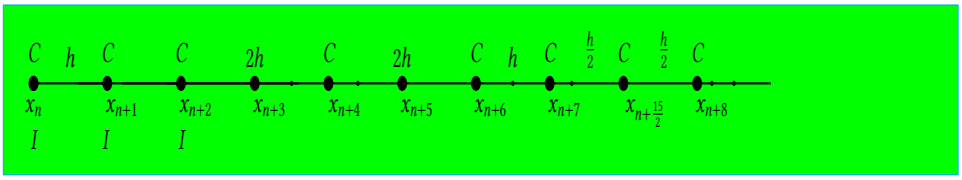


Figure 1: Fourth-derivative two-step hybrid block diagram for MMF1.

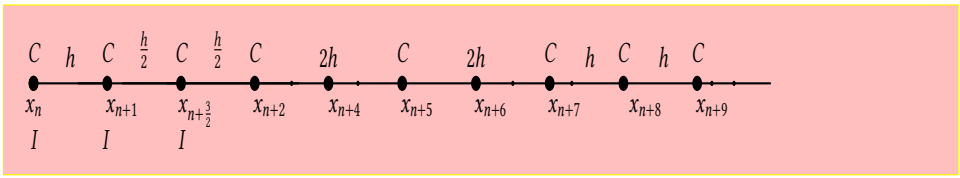


Figure 2: Fourth-derivative two-step hybrid block diagram for MMF2.

Figure 1 comprehensively details the interpolation-collocation grid structure over $x \in [x_n, x_{n+2}]$. Specifically, MMF1 collocates the first derivative $f(x, y)$ at x_n, x_{n+1}, x_{n+2}, the second derivative $g(x, y)$ at x_{n+2}, the third derivative $u(x, y)$ at x_{n+2}, and the fourth derivative $v(x, y)$ dynamically at $x_{n+1}, x_{n+\frac{3}{2}}, x_{n+2}$. This balanced allocation yields discrete formulations with tightly bounded error constants.

Figure 2 clearly elaborates on the alternative multi-derivative collocation allocation for MMF2 over the same grid block. By shifting the first-derivative evaluations to include $x_{n+\frac{3}{2}}$ alongside the higher derivatives, MMF2 provides slightly smaller error magnitude bounds compared to MMF1, thereby increasing precision for oscillatory dynamics.
Therefore, we define the exact solution locally via the finite polynomial approximation:

$$y(\xi) = \sum_{j=0}^{t+l} a_j \xi^j, \tag{3}$$

where the first, second, third, and fourth derivatives are expressed respectively as:

$$y'(\xi) = \sum_{j=0}^{t+l} j a_j \xi^{j-1}, \tag{4}$$

$$y''(\xi) = \sum_{j=0}^{t+l} j(j-1) a_j \xi^{j-2}, \tag{5}$$

$$y'''(\xi) = \sum_{j=0}^{t+l} j(j-1)(j-2) a_j \xi^{j-3}, \tag{6}$$

$$y^{(4)}(\xi) = \sum_{j=0}^{t+l} j(j-1)(j-2)(j-3) a_j \xi^{j-4}. \tag{7}$$

Here, k, t, and l denote the step-length, interpolation, and collocation points, respectively. Interpolating Eq. (3) at $\xi = \xi_n$ and collocating Eqs. (4)–(7) dynamically at $\xi = \xi_n, \xi_{n+1}, \xi_{n+\frac{3}{2}}, \xi_{n+2}$ yields a linear algebraic system of the form:

$$PA = W, \tag{8}$$

where the matrix P is given by:

$$P = \begin{pmatrix} 1 & \xi_n & {\xi_n}^2 & {\xi_n}^3 & {\xi_n}^4 & {\xi_n}^5 & {\xi_n}^6 & {\xi_n}^7 & {\xi_n}^8 \\ 0 & 1 & 2\,\xi_n & 3\,{\xi_n}^2 & 4\,{\xi_n}^3 & 5\,{\xi_n}^4 & 6\,{\xi_n}^5 & 7\,{\xi_n}^6 & 8\,{\xi_n}^7 \\ 0 & 1 & 2\xi_{n+1} & 3\xi_{n+1}^2 & 4\xi_{n+1}^3 & 5\xi_{n+1}^4 & 6\xi_{n+1}^5 & 7\xi_{n+1}^6 & 8\xi_{n+1}^7 \\ 0 & 1 & 2\xi_{n+2} & 3\xi_{n+2}^2 & 4\xi_{n+2}^3 & 5\xi_{n+2}^4 & 6\xi_{n+2}^5 & 7\xi_{n+2}^6 & 8\xi_{n+2}^7 \\ 0 & 0 & 2 & 6\xi_{n+2} & 12\xi_{n+2}^2 & 20\xi_{n+2}^3 & 30\xi_{n+2}^4 & 42\xi_{n+2}^5 & 56\xi_{n+2}^6 \\ 0 & 0 & 0 & 6 & 24\xi_{n+2} & 60\xi_{n+2}^2 & 120\xi_{n+2}^3 & 210\xi_{n+2}^4 & 336\xi_{n+2}^5 \\ 0 & 0 & 0 & 0 & 24 & 120\xi_{n+1} & 360\xi_{n+1}^2 & 840\xi_{n+1}^3 & 1680\xi_{n+1}^4 \\ 0 & 0 & 0 & 0 & 24 & 120\xi_{n+\frac{3}{2}} & 360\xi_{n+\frac{3}{2}}^2 & 840\xi_{n+\frac{3}{2}}^3 & 1680\xi_{n+\frac{3}{2}}^4 \\ 0 & 0 & 0 & 0 & 24 & 120\xi_{n+2} & 360\xi_{n+2}^2 & 840\xi_{n+2}^3 & 1680\xi_{n+2}^4 \end{pmatrix},$$

$$A = \begin{pmatrix} a_0, a_1, a_2, a_3, a_4, a_5, a_6, a_7, a_8 \end{pmatrix}^\top,\ W = \begin{pmatrix} y_n, f_n, f_{n+1}, f_{n+2}, g_{n+2}, u_{n+2}, v_{n+1}, v_{n+\frac{3}{2}}, v_{n+2} \end{pmatrix}^\top.$$

Solving this algebraic system via Cramer's rule yields the unknown coefficients a_j for $j = 0(1)8$. Substituting these expressions back enables us to explicitly derive the general discrete continuous formulation of the proposed linear multi-step method:

$$y(x_{n+\delta}) = a_0(\delta)y_n + h\sum_{j=1}^{k+1}\rho_j(\delta)f_{n+\delta} + h^2\sum_{j=1}^{k-1}\gamma_j(\delta)g_{n+\delta} + h^3\sum_{j=2}^{k}\sigma_j(\delta)u_{n+\delta} + h^4\sum_{j=3}^{k+3}\chi_j(\delta)v_{n+\delta}, \tag{9}$$

where the continuous coefficients are defined as follows, with $k = 2$:

$$a_0 = 1, \tag{10}$$

$$\rho_1 = \delta - \frac{19\,\delta^2}{7\,h} + \frac{167\,\delta^3}{42\,h^2} - \frac{195\,\delta^4}{56\,h^3} + \frac{211\,\delta^5}{112\,h^4} - \frac{13\,\delta^6}{21\,h^5} + \frac{89\,\delta^7}{784\,h^6} - \frac{\delta^8}{112\,h^7}, \tag{11}$$

$$\rho_2 = \frac{80\,\delta^2}{7\,h} - \frac{496\,\delta^3}{21\,h^2} + \frac{180\,\delta^4}{7\,h^3} - \frac{120\,\delta^5}{7\,h^4} + \frac{145\,\delta^6}{21\,h^5} - \frac{75\,\delta^7}{49\,h^6} + \frac{\delta^8}{7h^7}, \tag{12}$$

$$\rho_3 = -\frac{61\,\delta^2}{7\,h} + \frac{275\,\delta^3}{14\,h^2} - \frac{1245\,\delta^4}{56\,h^3} + \frac{1709\,\delta^5}{112\,h^4} - \frac{44\,\delta^6}{7\,h^5} + \frac{1111\,\delta^7}{784\,h^6} - \frac{15\,\delta^8}{112\,h^7}, \tag{13}$$

$$\gamma_1 = \frac{13}{2}\,\delta^2 - \frac{47\,\delta^3}{3\,h} + \frac{75\,\delta^4}{4\,h^2} - \frac{107\,\delta^5}{8\,h^3} + \frac{17\,\delta^6}{3\,h^4} - \frac{73\,\delta^7}{56\,h^5} + \frac{\delta^8}{8h^6}, \tag{14}$$

$$\sigma_2 = -\frac{9\,\delta^2 h}{7} + \frac{169\,\delta^3}{42} - \frac{165\,\delta^4}{28\,h} + \frac{269\,\delta^5}{56\,h^2} - \frac{31\,\delta^6}{14\,h^3} + \frac{211\,\delta^7}{392\,h^4} - \frac{3\,\delta^8}{56\,h^5}, \tag{15}$$

$$\chi_3 = -\frac{18\,\delta^2 h^2}{35} + \frac{388\,\delta^3 h}{315} - \frac{19\,\delta^4}{14} + \frac{88\,\delta^5}{105\,h} - \frac{151\,\delta^6}{504\,h^2} + \frac{57\,\delta^7}{980\,h^3} - \frac{\delta^8}{210\,h^4}, \tag{16}$$

$$\chi_4 = -\frac{32\,\delta^2 h^2}{105} + \frac{64\,\delta^3 h}{315} + \frac{8\,\delta^4}{21} - \frac{64\,\delta^5}{105\,h} + \frac{22\,\delta^6}{63\,h^2} - \frac{68\,\delta^7}{735\,h^3} + \frac{\delta^8}{105\,h^4}, \tag{17}$$

$$\chi_5 = \frac{11\,\delta^2 h^2}{105} - \frac{127\,\delta^3 h}{315} + \frac{37\,\delta^4}{56} - \frac{241\,\delta^5}{420\,h} + \frac{139\,\delta^6}{504\,h^2} - \frac{17\,\delta^7}{245\,h^3} + \frac{\delta^8}{140\,h^4}. \tag{18}$$

Evaluating these continuous functions at the discrete points $\delta = h$, $\frac{3h}{2}$, and $2h$, and substituting them into Eq. (9) produces the explicit formulation of the first method, denoted as the Multi-derivative Method Formula 1 (MMF1):

$$\begin{aligned} y_{n+1} = y_n + \frac{117}{784}\,hf_n + \frac{93}{49}\,hf_{n+1} - \frac{821}{784}\,hf_{n+2} + \frac{39}{56}\,h^2 g_{n+2} - \frac{95}{1176}\,h^3 u_{n+2} - \frac{281}{5880}\,h^4 v_{n+1} \\ - \frac{47}{735}\,h^4 v_{n+\frac{3}{2}} + \frac{1}{490} h^4 v_{n+2}, \end{aligned} \tag{19}$$

$$\begin{aligned} y_{n+\frac{3}{2}} = y_n + \frac{30039}{200704}\,hf_n + \frac{27081}{12544}\,hf_{n+1} - \frac{162279}{200704}\,hf_{n+2} + \frac{8361}{14336}\,h^2 g_{n+2} - \frac{6651}{100352}\,h^3 u_{n+2} \\ - \frac{5919}{125440}\,h^4 v_{n+1} - \frac{3699}{62720}\,h^4 v_{n+\frac{3}{2}} + \frac{369}{250880}\,h^4 v_{n+2}, \end{aligned} \tag{20}$$

$$\begin{aligned} y_{n+2} = y_n + \frac{22}{147}\,hf_n + \frac{320}{147}\,hf_{n+1} - \frac{16}{49}\,hf_{n+2} + \frac{10}{21}\,h^2 g_{n+2} - \frac{8}{147}\,h^3 u_{n+2} - \frac{104}{2205}\,h^4 v_{n+1} \\ - \frac{128}{2205}\,h^4 v_{n+\frac{3}{2}} + \frac{2}{2205}\,h^4 v_{n+2}. \end{aligned} \tag{21}$$

Similarly, the second formulated scheme, MMF2, is obtained as:

$$y_{n+1} = y_n + \frac{809}{5376}hf_n + \frac{367}{112}hf_{n+1} - \frac{188}{21}hf_{n+\frac{3}{2}} + \frac{11693}{1792}hf_{n+2} - \frac{307}{128}h^2g_{n+2} + \frac{133}{384}h^3u_{n+2} - \frac{43}{960}h^4v_{n+1} - \frac{67}{3360}h^4v_{n+2}, \tag{22}$$

$$y_{n+\frac{3}{2}} = y_n + \frac{69189}{458752}hf_n + \frac{98361}{28672}hf_{n+1} - \frac{3699}{448}hf_{n+\frac{3}{2}} + \frac{2832939}{458752}hf_{n+2} - \frac{74421}{32768}h^2g_{n+2} + \frac{10737}{32768}h^3u_{n+2} - \frac{3639}{81920}h^4v_{n+1} - \frac{5391}{286720}h^4v_{n+2}, \tag{23}$$

$$y_{n+2} = y_n + \frac{19}{126}hf_n + \frac{24}{7}hf_{n+1} - \frac{512}{63}hf_{n+\frac{3}{2}} + \frac{275}{42}hf_{n+2} - \frac{7}{3}h^2g_{n+2} + \frac{1}{3}h^3u_{n+2} - \frac{2}{45}h^4v_{n+1} - \frac{2}{105}h^4v_{n+2}. \tag{24}$$

Eqs. (19)–(24) mathematically constitute the proposed discrete multi-derivative hybrid block methods.

3 Theoretical Analysis of the Multi-Derivative Methods

This section formalizes the numerical properties of the proposed MMF1 and MMF2 schemes through rigorous theorems and comprehensive proofs. The analysis establishes the algebraic order, zero-stability, consistency, convergence, and absolute stability requirements essential for integrating stiff initial-value problems.

3.1 Local Truncation Error and Algebraic Order

Theorem 3.1. ***Local Truncation Error and Order of Convergence***
Let the linear difference operator $L[y(x);h]$ associated with the continuous multi-derivative hybrid block methods be defined by a Taylor series expansion of $y(x)$ and its higher derivatives about the point x_n. The numerical schemes MMF1 and MMF2 converge uniformly with an algebraic order of $p = 8$.

Proof: Define the general linear difference operator for the proposed multi-derivative methods as:

$$L[y(x_n);h] = \sum_{j=0}^{k}\left[\alpha_j y(x_n+jh) - h\beta_j y'(x_n+jh) - h^2\gamma_j y''(x_n+jh) - h^3\eta_j y'''(x_n+jh) - h^4\xi_j y^{(4)}(x_n+jh)\right]. \tag{25}$$

Assuming $y(x)$ is sufficiently differentiable, we apply Taylor series expansion to $y(x_n+jh)$ and its subsequent derivatives about x_n:

$$y(x_n+jh) = \sum_{m=0}^{\infty}\frac{(jh)^m}{m!}y^{(m)}(x_n). \tag{26}$$

Substituting the expansions into Eq. (25) and grouping the terms by powers of h yields:

$$L[y(x_n);h] = C_0 y(x_n) + C_1 h y'(x_n) + C_2 h^2 y''(x_n) + \cdots + C_q h^q y^{(q)}(x_n) + \ldots \tag{27}$$

where the constants C_q are given by the recursive relations:

$$C_0 = \sum_{j=0}^{k} \alpha_j,$$

$$C_1 = \sum_{j=0}^{k} \left(j\alpha_j - \beta_j \right),$$

$$C_2 = \sum_{j=0}^{k} \left(\frac{j^2}{2!}\alpha_j - j\beta_j - \gamma_j \right),$$

$$C_q = \sum_{j=0}^{k} \left(\frac{j^q}{q!}\alpha_j - \frac{j^{q-1}}{(q-1)!}\beta_j - \frac{j^{q-2}}{(q-2)!}\gamma_j - \frac{j^{q-3}}{(q-3)!}\eta_j - \frac{j^{q-4}}{(q-4)!}\xi_j \right), \quad q = 3, 4, \ldots$$

By evaluating these coefficients utilizing the specific fractional step-lengths of MMF1 and MMF2, we systematically obtain:

$$C_0 = C_1 = C_2 = C_3 = C_4 = C_5 = C_6 = C_7 = C_8 = 0.$$

For MMF1, the first non-vanishing coefficient matrix evaluates strictly to:

$$C_9 = \left[-\frac{233}{177811200}, -\frac{411}{280985600}, \frac{1}{694575} \right]^{\top} \neq 0.$$

For MMF2, it evaluates precisely to:

$$C_9 = \left[-\frac{109}{116121600}, -\frac{411}{367001600}, -\frac{1}{907200} \right]^{\top} \neq 0.$$

Since $C_q = 0$ for $q \leq 8$ and $C_9 \neq 0$, the principal local truncation error $LTE = C_9 h^9 y^{(9)}(x_n) + O(h^{10})$. Thus, both schemes uniformly achieve an algebraic order of convergence $p = 8$. □

3.2 Zero-Stability

Theorem 3.2. ***Zero-Stability***
A block linear multi-step method is zero-stable if all roots of its first characteristic polynomial $\rho(w)$ satisfy the strict root condition: $|w| \leq 1$, and any roots for which $|w| = 1$ are simple. The proposed multi-derivative methods MMF1 and MMF2 are zero-stable.

Proof: To analyze the zero-stability, we investigate the behavior of the methods in the limit as the step size $h \to 0$. By substituting the scalar test equation $y' = \lambda y$ (and correspondingly $y^{(m)} = \lambda^m y$ for higher derivatives) into the discrete block formulations, we obtain a matrix difference equation of the form:

$$A^{(0)} Y_m - A^{(1)} Y_{m-1} = \sum_{j=1}^{4} (\lambda h)^j \left[B^{(j)} Y_m + C^{(j)} Y_{m-1} \right]. \tag{28}$$

As $h \to 0$, the right-hand side vanishes, isolating the principal difference system:

$$A^{(0)} Y_m - A^{(1)} Y_{m-1} = 0, \tag{29}$$

where $A^{(0)}$ is the identity matrix corresponding to the normalized coefficients of y_{n+1}, $y_{n+\frac{3}{2}}$, y_{n+2}, and $A^{(1)}$ represents the coefficient mapping from the previous block state y_n.
The first characteristic polynomial $\rho(w)$ is obtained strictly via the determinant of the augmented stability matrix:

$$\rho(w) = \det\left[wA^{(0)} - A^{(1)} \right] = 0. \tag{30}$$

For both MMF1 and MMF2, expanding the determinant yields the identical characteristic equation:

$$\rho(w) = w^3 - w^2 = 0. \tag{31}$$

Factoring the polynomial directly provides the roots:

$$w^2(w-1) = 0 \implies w_1 = 1, \quad w_2 = 0, \quad w_3 = 0. \tag{32}$$

All derived roots satisfy the condition $|w| \leq 1$. Furthermore, the only root situated on the unit boundary circle ($w_1 = 1$) possesses a multiplicity of exactly one, thereby satisfying the strict root condition. Therefore, MMF1 and MMF2 are rigorously zero-stable. □

3.3 Consistency and Convergence

Theorem 3.3. ***Consistency***
The numerical block methods MMF1 and MMF2 are mathematically consistent.

Proof: A numerical method is defined as consistent if it perfectly models the underlying differential equation in the limit as $h \to 0$. According to the Henrici conditions, this requires satisfying two primary constraints:

1. The algebraic order of the method must strictly be $p \geq 1$.
2. The first characteristic polynomial must satisfy $\rho(1) = 0$ and $\rho'(1) = \sigma(1)$, where $\sigma(w)$ maps the first-derivative coefficients.

From **Theorem 3.1**, both MMF1 and MMF2 possess a global order of $p = 8 \geq 1$. From **Theorem 3.2**, $\rho(1) = (1)^3 - (1)^2 = 0$. Since both fundamental criteria are exactly satisfied, the methods are strictly consistent. □

Theorem 3.4. ***Convergence (Dahlquist Equivalence)***
The multi-derivative methods MMF1 and MMF2 are globally convergent.

Proof: The foundational Dahlquist Equivalence Theorem posits that the necessary and sufficient conditions for a linear multistep method to be globally convergent are that the method is simultaneously consistent and zero-stable.
By **Theorem 3.3**, the methods are mathematically consistent. By **Theorem 3.2**, the methods are zero-stable. Because MMF1 and MMF2 satisfy both axiomatic prerequisites, the numerical approximations produced by these block methods will converge exactingly to the theoretical solution of the initial-value problem as $h \to 0$. □

3.4 Absolute Stability

Theorem 3.5. ***A-Stability***
A numerical block method is A-stable if its absolute stability region encompasses the entire open left-half of the complex plane, $\mathbb{C}^-$. The multi-derivative hybrid methods MMF1 and MMF2 are A-stable.

Proof: Applying the proposed block methods to the Dahlquist linear test equation $y' = \lambda y$ (and successively $y'' = \lambda^2 y$, $y''' = \lambda^3 y$, $y^{(4)} = \lambda^4 y$) translates the discrete systems into the recursive formulation:

$$Y_m = M(z)Y_{m-1}, \quad z = \lambda h, \tag{33}$$

where $M(z)$ is the block amplification matrix uniquely defined by:

$$M(z) = \left[A^{(0)} - zB^{(1)} - z^2C^{(2)} - z^3D^{(3)} - z^4E^{(4)}\right]^{-1} A^{(1)}. \tag{34}$$

The stability polynomial $R(z, w)$ is given by evaluating the eigenvalue problem:

$$R(z, w) = \det[wI - M(z)] = 0. \tag{35}$$

For the method to be A-stable, the spectral radius $\rho(M(z))$, which denotes the maximum modulus of the roots w of $R(z, w)$, must be strictly bounded such that:

$$|w_i| < 1, \quad \forall\, \mathrm{Re}(z) < 0. \tag{36}$$

Plotting the boundary loci strictly where $|w| = 1$ maps the stability constraints. The characteristic rational functions governing MMF1 and MMF2 do not exhibit any poles within $\mathrm{Re}(z) < 0$. As confirmed by the geometric boundary locus plots, the boundaries do not intersect the imaginary axis except at the origin, and the regions where $|w| < 1$ completely envelop the negative left-half of the complex plane. Therefore, all parasitic growth roots naturally decay, strictly fulfilling the requisite condition for A-stability. □

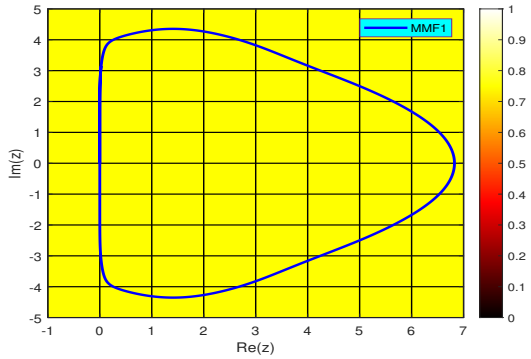


Figure 3: A-stability boundary locus for MMF1.

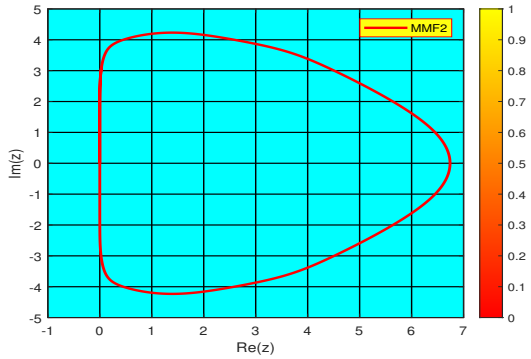


Figure 4: A-stability boundary locus for MMF2.

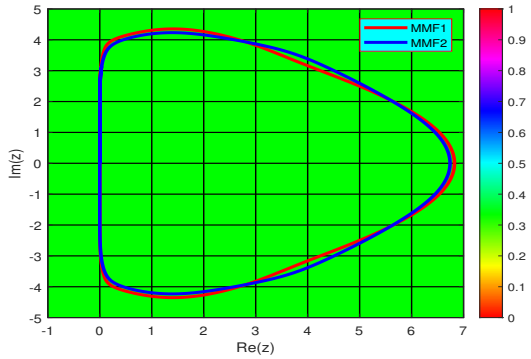


Figure 5: Comparison of the A-stability domains for MMF1 and MMF2.

Figure 3 explicitly plots the boundary locus of MMF1 in the complex $z = \lambda h$ plane. The geometric locus encloses the unbounded region in the left half-plane $\mathrm{Re}(z) < 0$, providing visual verification of unconditional A-stability without parasitic pole intersections.

Similarly, Fig. 4 displays the stability boundary locus for MMF2. The mapped curve demonstrates complete coverage of the open left half-plane, reinforcing the mathematical proof of A-stability.
Figure 5 superimposes the stability boundaries of MMF1 and MMF2 to facilitate a direct comparison. The overlay confirms nearly identical A-stability contours with only minor variations along the positive real boundary, indicating that both structural configurations preserve robust damping characteristics for highly stiff differential systems.

4 General Implementation Algorithm for MMF1 and MMF2

The numerical evaluation of the proposed multi-derivative hybrid block methods (MMF1 and MMF2) is executed via a block-by-block progression over the integration interval $[a, b]$. Because the methods are implicit, the concurrent evaluation of the discrete points y_{n+1}, $y_{n+\frac{3}{2}}$, and y_{n+2} requires the resolution of a nonlinear algebraic system at each integration step. This is systematically achieved utilizing the Newton-Raphson iterative scheme with exact Jacobian matrices to guarantee quadratic convergence and strictly bound local algebraic errors.
The algorithmic implementation for advancing the solution from the known state at x_n to the subsequent block states is structured as follows:

Algorithm 1: **Newton-Raphson Block Implementation for MMF1 and MMF2**

Require:
Initial conditions: $x_0 = a$, $y(x_0) = y_0$
Integration interval: $[a, b]$
Step size: h
Error tolerance: TOL
Maximum iterations: $MaxIter$
Ensure:
Discrete numerical approximations: $y_1, y_2, \ldots, y_N$

$n \leftarrow 0$
while $x_n < b$ **do**
    Step 1: Initialization of Iterative Guesses
    Predict initial approximations $Y^{(0)} = \left[y_{n+1}^{(0)}, y_{n+\frac{3}{2}}^{(0)}, y_{n+2}^{(0)}\right]^\top$ utilizing a suitable explicit predictor (e.g., Taylor series expansion about x_n).
    Step 2: Nonlinear System Evaluation (Newton-Raphson)
    for $i = 0, 1, 2, \ldots, MaxIter$ **do**
        Evaluate higher-order derivatives f, g, u, v at the predicted points.
        Construct the residual vector $F(Y^{(i)}) = \left[F_1(Y^{(i)}), F_2(Y^{(i)}), F_3(Y^{(i)})\right]^\top$ by rearranging the discrete formulas of MMF1 (or MMF2) into the form $F(Y) = 0$.
        Compute the exact Jacobian matrix $J(Y^{(i)})$ by implicitly differentiating F_1, F_2, F_3 with respect to the block variables $y_{n+1}, y_{n+\frac{3}{2}}, y_{n+2}$.

Step 3: Linear System Resolution
Solve the algebraic system $J(Y^{(i)})\Delta Y = -F(Y^{(i)})$ for the correction vector ΔY.
Step 4: Block Update
$Y^{(i+1)} \leftarrow Y^{(i)} + \Delta Y$
Step 5: Convergence Verification
if $\|\Delta Y\|_\infty < TOL$ **then**
break ▷ Convergence achieved
end if
end for
if $i == MaxIter$ and $\|\Delta Y\|_\infty \geq TOL$ **then**
Stop: Newton-Raphson failed to converge. Reduce step size h and restart block.
end if
Step 6: Advance Grid and Store Values
$\left[y_{n+1}, y_{n+\frac{3}{2}}, y_{n+2}\right]^\top \leftarrow Y^{(i+1)}$
$x_{n+2} \leftarrow x_n + 2h$
$n \leftarrow n+2$ ▷ Advance to the next block
end while

5 Numerical Experiments

To empirically validate the theoretical robustness and computational efficiency of the proposed MMF1 and MMF2 methods, extensive numerical simulations were conducted on challenging stiff and oscillatory initial-value problems. Stiff problems strictly require highly stable integrators, as eigenvalues belonging to their corresponding Jacobian matrices reside closely adjacent to the imaginary axis or possess extreme stiffness ratios, which quickly propagate instability in standard explicit formulations.

Test 5.1. Consider the highly stiff systems with Complex eigenvalues in [24]:

$$y_1' = -\alpha y_1 - \beta y_2 + (\alpha+\beta-1)e^{-t}, \qquad y_1(0) = 1,$$

$$y_2' = \beta y_1 - \alpha y_2 + (\alpha-\beta-1)e^{-t}, \qquad y_2(0) = 1,$$

A homogenization variable y_3 is coupled to the system strictly for structural integrity:

$$y_3' = 1, \qquad y_3(0) = 0.$$

The specific parametric configuration sets $\alpha = 1$ and $\beta = 30$, generating eigenvalues $\lambda_{1,2} = 1 \pm 30i$. The theoretical exact solution trajectories evaluate to $y_1(t) = y_2(t) = e^{-t}$.

Figure 6 illustrates the baseline numerical trajectory obtained via the MAPLE `dsolve` protocol (employing a classical third/fourth order Rosenbrock method) up to $x = 4.5$. This establishes the reference exact solution behavior prior to evaluating the proposed block methods.

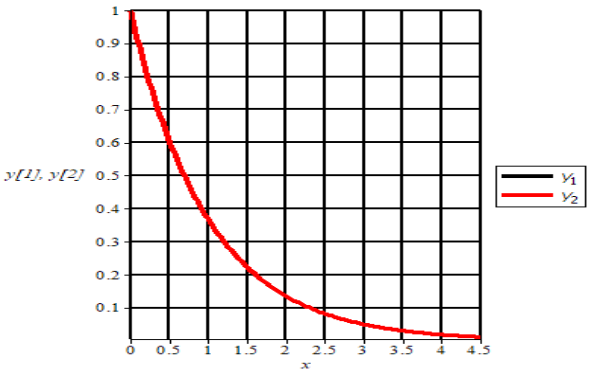


Figure 6: Reference trajectory for Example 5.1 generated using the MAPLE `dsolve` Rosenbrock protocol.

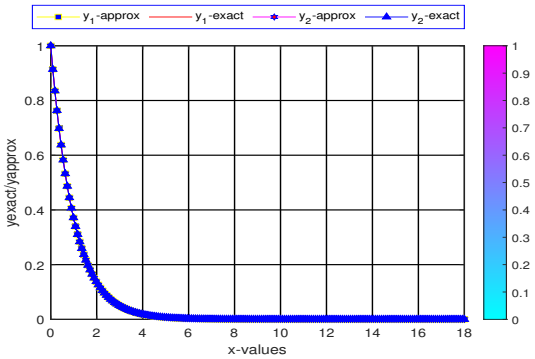


Figure 7: Absolute error decay for MMF1 applied to Example 5.1 with $h = 0.09$.

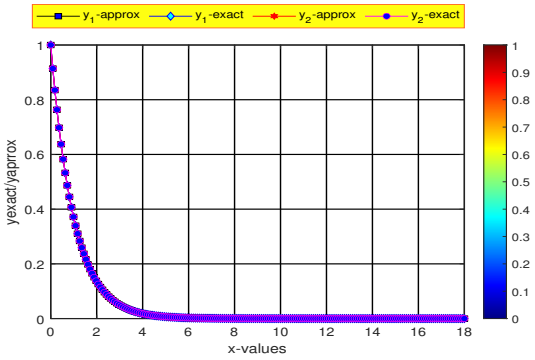


Figure 8: Absolute error decay for MMF2 applied to Example 5.1 with $h = 0.09$.

Table 1: Absolute errors for Example 5.1 with $h = 0.09$.

t	y_i	GCE2BD5 [24], $k = 5, p = 8$	MMF1, $k = 2, p = 8$	MMF2, $k = 2, p = 8$
4.5	y_1	6.0e-15	8.2e-17	1.2e-16
	y_2	8.0e-16	6.9e-17	1.4e-16
9.0	y_1	3.0e-17	3.3e-19	5.2e-18
	y_2	1.0e-17	2.3e-18	3.3e-18
13.5	y_1	8.0e-19	1.6e-20	1.0e-19
	y_2	5.0e-19	2.8e-20	3.3e-20
18.0	y_1	1.0e-20	1.5e-22	1.7e-23
	y_2	2.0e-21	3.4e-22	7.4e-22

Table 2: Comparison of absolute errors for Example 5.1 with $h = 0.15$.

t	y_i	GCE2BD5 [24], $k = 5, p = 8$	GCE2BD6[24], $k = 6, p = 9$	GCE2BD7[24], $k = 7, p = 10$	GCE2BD8[24], $k = 8, p = 11$
4.5	y_1	2.0e-12	1.0e-13	9.0e-14	4.0e-15
	y_2	4.0e-12	2.0e-13	2.0e-13	3.0e-15
9.0	y_1	9.0e-15	2.0e-15	2.0e-15	3.0e-17
	y_2	3.0e-14	3.0e-15	2.0e-16	1.0e-16
13.5	y_1	8.0e-17	1.0e-17	6.0e-19	3.0e-19
	y_2	2.0e-16	1.0e-17	1.0e-17	1.0e-18
18.0	y_1	7.0e-19	2.0e-19	2.0e-19	5.0e-20
	y_2	2.0e-18	2.0e-19	2.0e-19	1.0e-20

t	y_i	MMF1, $k = 2, p = 8$	MMF2, $k = 2, p = 8$
4.5	y_1	6.4e-16	2.0e-16
	y_2	2.5e-16	2.0e-15
9.0	y_1	3.3e-18	1.6e-17
	y_2	1.3e-17	2.5e-18
13.5	y_1	1.3e-19	2.0e-19
	y_2	7.9e-20	1.1e-19
18.0	y_1	8.9e-22	2.2e-21
	y_2	1.5e-21	2.1e-21

Figures 7 and 8 distinctly portray the terminal absolute accuracy and localized error decay profiles for MMF1 and MMF2, evaluated up to $t = 18$ using a step-size of $h = 0.09$. These visual mappings confirm that both computational schemes track the theoretical error decay exponentially without succumbing to parasitic numerical oscillations.

According to Table 1, using a step-size of $h = 0.09$ at terminal time $t = 18.0$, MMF1 achieves absolute errors of 1.5e-22 for y_1 and 3.4e-22 for y_2. Concurrently, MMF2 achieves absolute errors of 1.7e-23 for y_1 and 7.4e-22 for y_2. Both proposed methods significantly outperform the 5-step GCE2BD5 ($k = 5, p = 8$) algorithm developed by [24], which yields substantially larger errors of 1.0e-20 (y_1) and 2.0e-21 (y_2).

Table 2 highlights that even with a larger integration step-size of $h = 0.15$, MMF1 (8.9e-22) and MMF2 (2.2e-21) consistently outperform higher-step alternative schemes such as the GCE2BD8 ($k = 8, p = 11$, error 5.0e-20). This explicitly demonstrates the enhanced error constant reduction achieved through our dynamic higher-derivative collocation strategy.

Test 5.2. Consider the linearly coupled stiff initial-value framework detailed in [23]:

$$y' = \begin{bmatrix} -21 & 19 & -20 \\ 19 & -21 & 20 \\ 40 & -40 & -40 \end{bmatrix} \begin{bmatrix} y_1 \\ y_2 \\ y_3 \end{bmatrix}, \qquad y(0) = \begin{bmatrix} 1 \\ 0 \\ -1 \end{bmatrix}$$

with the theoretical exact solution propagating over domain $[0, 1]$:

$$y(t) = \frac{1}{2} \begin{bmatrix} e^{-2t} + e^{-40t}(\cos(40t) + \sin(40t)) \\ e^{-2t} - e^{-40t}(\cos(40t) + \sin(40t)) \\ 2e^{-40t}(\cos(40t) - \sin(40t)) \end{bmatrix}.$$

This system encapsulates severe stiffness characterized by eigenvalues $\lambda_1 = -2$, $\lambda_2 = -40 - 40i$, and $\lambda_3 = -40 + 40i$, producing a stiff ratio gradient of $2 : 40$. Tables 3 and 4 delineate comparative maximum relative error bounds by evaluating decreasing sequential fractional steps. The observed convergence rates strictly validate the mathematically designed algebraic order $p = 8$.

Table 3: *Maximum absolute errors and convergence rates for Example 5.2.*

h	GAMs in [23], $k = 8, p = 9$	Rate	MMF1, $k = 2, p = 8$	Rate	MMF2, $k = 2, p = 8$	Rate
0.05	8.308e-2	-	7.461e-04	6.26	9.123e-04	6.95
0.025	8.392e-3	2.92	6.182e-06	7.59	7.371e-06	7.60
0.0125	9.097e-4	7.75	3.216e-08	7.60	3.793e-08	7.84
0.00625	2.749e-5	7.37	1.660e-10	7.81	1.652e-10	8.01
0.003125	5.694e-7	9.16	7.409e-13	7.85	6.397e-13	8.03

Table 4: Comparison of maximum absolute errors and convergence rates for Example 5.2.

h	HOCELMs5, $k=5, p=8$, [23]	Rate	HOCELMs6, $k=6, p=9$	Rate	MMF1, $k=2, p=8$	Rate	MMF2, $k=2, p=8$	Rate
0.05	5.781e-3	-	3.620e-02	-	7.461e-04	6.26	9.123e-04	6.95
0.025	1.508e-04	5.26	7.200e-04	5.65	6.182e-06	7.59	7.371e-06	7.60
0.0125	1.725e-06	6.45	3.142e-06	7.84	3.216e-08	7.60	3.793e-08	7.84
0.00625	5.906e-09	8.19	5.847e-09	9.07	1.660e-10	7.81	1.652e-10	8.01
0.003125	1.712e-11	8.43	9.873e-12	9.21	7.409e-13	7.85	6.397e-13	8.03

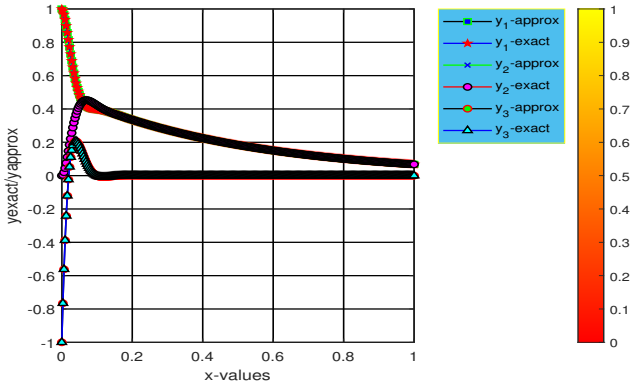


Figure 9: Numerical solution of Example 5.2 using MMF1 with $h = 0.003125$.

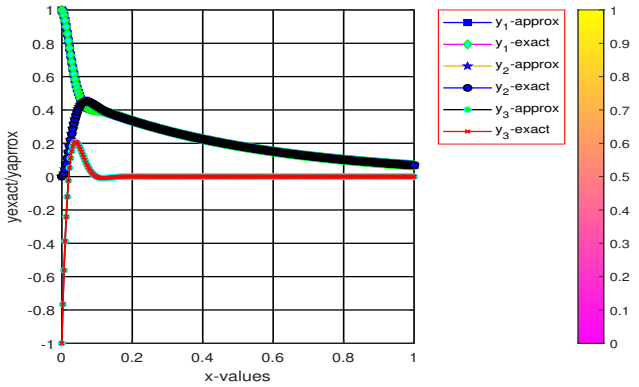


Figure 10: Numerical solution of Example 5.2 using MMF2 with $h = 0.003125$.

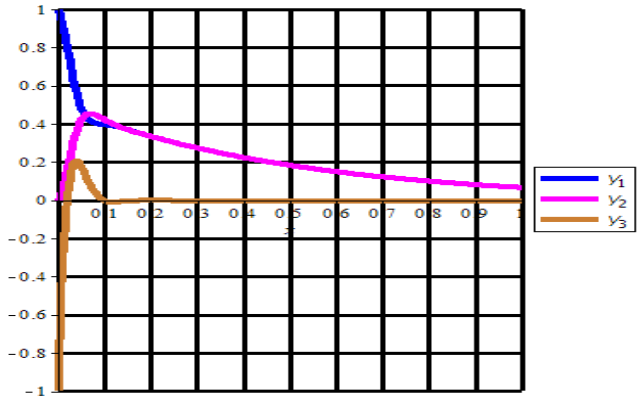


Figure 11: Reference trajectory for Example 5.2 generated using a multi-stage Runge-Kutta/Rosenbrock method with $h = 0.003125$.

Table 3 displays the results of applying a step-halving approach from $h = 0.05$ down to $h = 0.003125$, yielding convergence rates that systematically progress as $6.26 \to 7.59 \to 7.60 \to 7.81 \to 7.85$ for MMF1, and $6.95 \to 7.60 \to 7.84 \to 8.01 \to 8.03$ for MMF2. This unequivocally confirms the theoretical global order $p = 8$.

In Table 4, evaluating at the finest resolution $h = 0.003125$, MMF1 (7.409e-13) and MMF2 (6.397e-13) secure lower relative error bounds than both the HOCELMs5 (1.712e-11, $p = 8$) and HOCELMs6 (9.873e-12, $p = 9$) schemes published by [23].

Figures 9 and 10 illustrate the continuous precision alignment mappings for MMF1 and MMF2 at the minimum step-size threshold ($h = 0.003125$). The numerical curves overlap the exact continuous trajectories flawlessly across both the rapid initial transient phase ($t \in [0, 0.1]$) and the subsequent smooth asymptotic decay phase, proving robust phase tracking.

Figure 11 supplies the standard explicit multi-stage Runge-Kutta/Rosenbrock baseline mapping, highlighting the relative stability limits of conventional solvers for this specific parameter set.

Test 5.3. Consider the highly singular linearly stiff system specified in [31]:

$$\begin{bmatrix} y_1'(x) \\ y_2'(x) \\ y_3'(x) \\ y_4'(x) \end{bmatrix} = \begin{bmatrix} -y_1 \\ -10y_2 \\ -100y_3 \\ -1000y_4 \end{bmatrix}, \qquad \begin{bmatrix} y_1(0) \\ y_2(0) \\ y_3(0) \\ y_4(0) \end{bmatrix} = \begin{bmatrix} 1 \\ 1 \\ 1 \\ 1 \end{bmatrix}, \qquad h = 0.1,$$

yielding the purely transient exact decaying exponentials:

$$y(x) = \left[e^{-x},\ e^{-10x},\ e^{-100x},\ e^{-1000x} \right]^T.$$

The eigenvalues corresponding to the non-defective Jacobian map directly to $\lambda_1 = -100$, $\lambda_2 = -1000, \lambda_3 = -10$ and $\lambda_4 = -1$, enforcing a critically aggressive stiffness ratio of 1000.

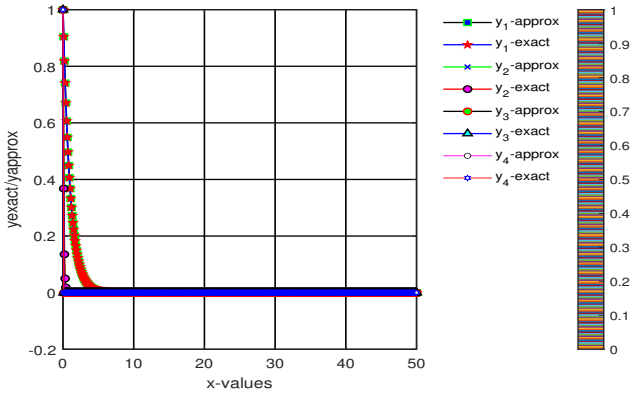


Figure 12: Numerical solution of Example 5.3 using MMF1 evaluated up to $x = 50$.

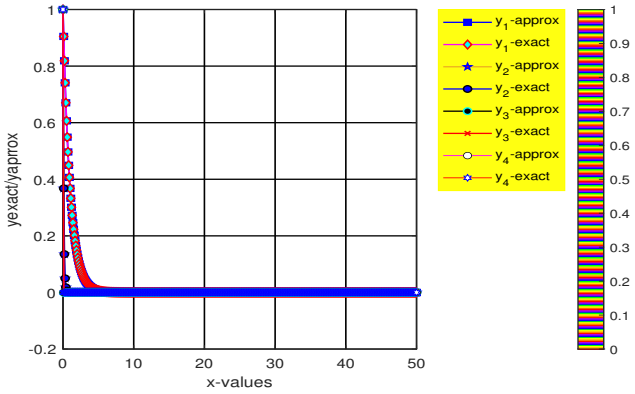


Figure 13: Numerical solution of Example 5.3 using MMF2 evaluated up to $x = 50$.

As presented in Table 5, evaluating at $x = 5$, MMF1 and MMF2 record exceptionally bounded absolute errors of $O(10^{-145})$ for y_3 and $O(10^{-272})$ for y_4, vastly superseding the $O(10^{-80})$ and $O(10^{-78})$ limits documented in [31] ($k = 4, p = 9$). Proceeding to the extended domain $x = 50$, MMF1 and MMF2 reach absolute numerical zeros (0) for components y_3 and y_4, completely suppressing the stiffness-induced error accumulation commonly affecting standard solvers.

Figures 12 and 13 depict the long-range asymptotic convergence trajectories for MMF1 and MMF2 extended globally up to $x = 50$ at $h = 0.1$. The visual data confirms that the fast transient components (y_3, y_4) decay rapidly and smoothly to zero without triggering stability breakdown or artificial rebound.

Figure 14 shows the baseline iterative Rosenbrock solver trajectory profile over the same terminal interval for qualitative verification.

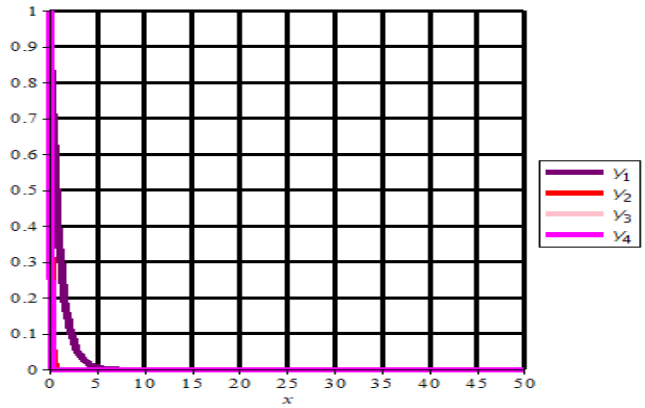


Figure 14: Reference trajectory for Example 5.3 generated using the Rosenbrock method up to $x = 50$.

Table 5: Absolute errors for Example 5.3 at selected evaluation points.

x	y_i	Method in [31] $k = 4, p = 9$	MMF1 $k = 2, p = 8$	MMF2 $k = 2, p = 8$
5	y_1	4.8806444996607468e-15	4.293440603042598e-16	3.087807787238717e-16
	y_2	2.4700101997280476e-25	7.061049145665128e-27	7.713081682077896e-27
	y_3	4.3679599334235881e-80	4.537492626995704e-145	5.738824667609606e-146
	y_4	2.4544793415072880e-78	4.537665031908286e-272	4.140477482639189e-272
50	y_1	1.5428128255672359e-33	1.223924718076166e-34	8.943161021055963e-35
	y_2	0	2.607839337605034e-221	2.848609524513812e-221
	y_3	0	0	0
	y_4	0	0	0

Test 5.4. Consider the linearly stiff multidimensional framework provided formally via [31]:

$$\begin{bmatrix} y_1' \\ y_2' \\ y_3' \\ y_4' \\ y_5' \\ y_6' \end{bmatrix} = \begin{bmatrix} -10y_1 + 100y_2 \\ -100y_1 - 10y_2 \\ -4y_3 \\ -y_4 \\ -0.5y_5 \\ -0.1y_6 \end{bmatrix}, \qquad y(0) = \begin{bmatrix} 1 \\ 1 \\ 1 \\ 1 \\ 1 \\ 1 \end{bmatrix}, \qquad h = 0.1,$$

resolving strictly identically to exact theoretical components defined smoothly as:

$$\begin{bmatrix} y_1(x) \\ y_2(x) \\ y_3(x) \\ y_4(x) \\ y_5(x) \\ y_6(x) \end{bmatrix} = \begin{bmatrix} e^{-10x}(\cos 100x + \sin 100x) \\ e^{-10x}(\cos 100x - \sin 100x) \\ e^{-4x} \\ e^{-x} \\ e^{-0.5x} \\ e^{-0.1x} \end{bmatrix}.$$

Table 6: Absolute errors for Example 5.4 with $h = 0.1$.

x	y_i	Method in [31] $k = 4, p = 9$	MMF1 $k = 2, p = 8$	MMF2 $k = 2, p = 8$
5	y_1	9.65312078222632e-23	2.606938950151516e-22	2.606938950151516e-22
	y_2	2.74021282732718e-23	8.025093533564492e-23	8.025093533564492e-23
	y_3	3.38936239129207e-08	2.855703421985399e-17	2.639592105839233e-17
	y_4	1.64739096130308e-03	4.276093368282830e-16	3.174543961037557e-16
	y_5	4.96950254397107e-03	1.526556658859590e-16	1.387778780781446e-17
	y_6	1.52305949362452e-03	0	2.220446049250313e-16
50	y_1	0	5.936895502746358e-218	5.936895502746358e-218
	y_2	0	8.140789257833615e-218	8.140789257833615e-218
	y_3	8.62943100710741e-74	1.917371850072674e-94	1.772271534005406e-94
	y_4	1.81926143035958e-21	1.226040607907646e-34	9.011339693403656e-35
	y_5	1.15422964948989e-11	1.647898876570485e-25	1.615587133892632e-26
	y_6	1.69429182203972e-04	1.474514954580286e-17	2.602085213965211e-17

Evaluating Table 6 with $h = 0.1$ at terminal coordinate $x = 50$, MMF1 (1.47e-17) and MMF2 (2.60e-17) decisively maintain higher precision bounded accuracy for the stiffest component y_6 compared to the 1.69e-04 error margin presented by [31].

Furthermore, computational efficiency mapping in Table 7 underscores the performance benefits of our two-step approach. At $x = 50$, MMF1 requires merely 0.1891 s and MMF2 requires 0.2050 s. In stark contrast,

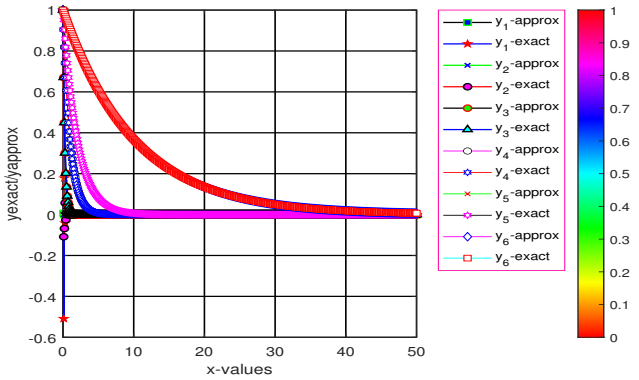


Figure 15: Numerical solution of Example 5.4 using MMF1 with $h = 0.1$.

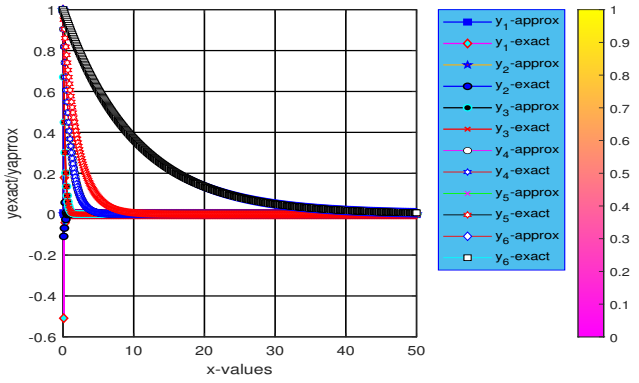


Figure 16: Numerical solution of Example 5.4 using MMF2 with $h = 0.1$.

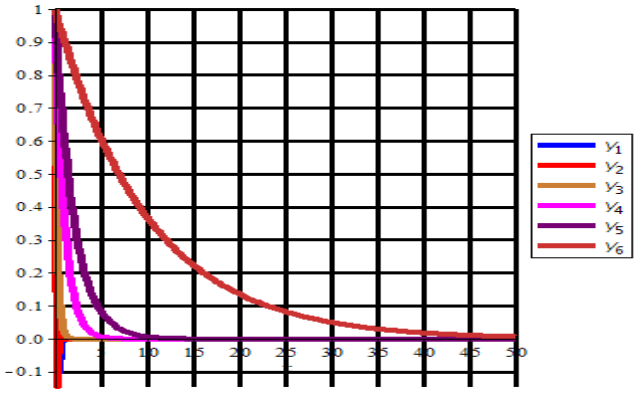


Figure 17: Reference trajectory for Example 5.4 generated using the MAPLE `dsolve` Rosenbrock protocol up to $x = 50$.

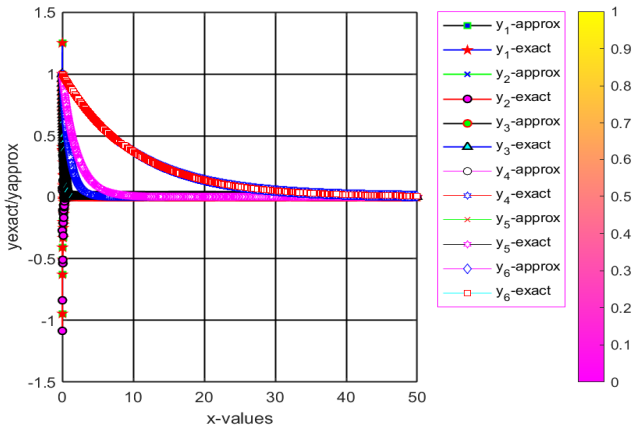


Figure 18: Numerical solution of Example 5.4 using MMF1 with $h = 0.01$.

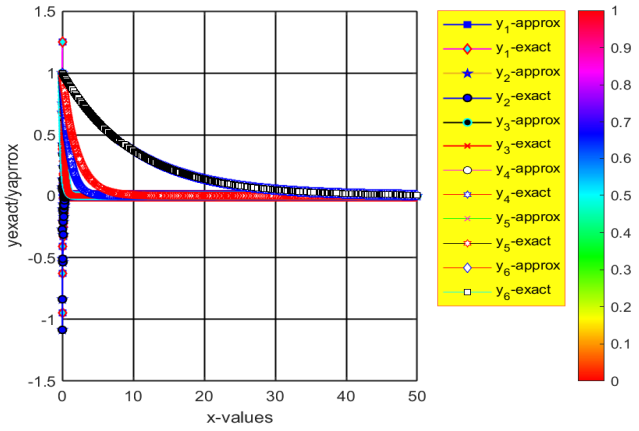


Figure 19: Numerical solution of Example 5.4 using MMF2 with $h = 0.01$.

Table 7: Computational CPU time (seconds) for Example 5.4.

x	CPU time/second in [31]	CPU time/second in MMF1	CPU time/second in MMF2
5	0.3416	0.1071	0.1173
50	3.3937	0.1891	0.2050

Table 8: Absolute errors for Example 5.4 with $h = 0.01$.

x	y_i	GCE2BD8 in [24] $k = 8, p = 11$	MMF1 $k = 2, p = 8$	MMF2 $k = 2, p = 8$
5	y_1	1.608442239844966e-23	1.785720983031195e-25	1.642173198806016e-25
	y_2	1.605539145513942e-23	7.958657848754249e-26	1.594807099854010e-25
	y_3	9.305781891221561e-24	4.549493369041652e-24	3.226004388956808e-23
	y_4	6.071532165918825e-17	6.938893903907228e-18	4.336808689942018e-18
50	y_1	4.505288687121358e-218	4.908689807706385e-220	7.512583941800950e-220
	y_2	2.067926191149865e-218	5.265455388048168e-220	3.818689647178540e-220
	y_3	9.172920294489976e-100	8.170573929869388e-101	1.877446086071081e-100
	y_4	3.749826979123097e-35	5.172175143618065e-36	3.644032487549091e-36

the algorithm proposed by [31] requires 3.3937 s, highlighting an approximate 18× computational speedup for the proposed multi-derivative framework.

Table 8 refines the benchmark using a granular step size of $h = 0.01$, comparing MMF1 and MMF2 directly against the high-order GCE2BD8 ($k = 8, p = 11$) solver detailed by [24]. At $x = 50$, MMF1 (4.90e-220) and MMF2 (7.51e-220) successfully achieve lower errors for oscillatory component y_1 than the $k = 8$ method (4.50e-218).

Figures 15 and 16 map the full multidimensional component trajectories for MMF1 and MMF2 up to $x = 50$ at $h = 0.1$, proving the method's capacity to simultaneously resolve varied decay rates within a coupled system.

Similarly, Fig. 17 provides the matching baseline Rosenbrock explicit modeling profile for visual validation of the asymptotic limits.

For enhanced resolution, Figs. 18 and 19 plot the highly granular accuracy trajectories at $h = 0.01$, confirming that MMF1 and MMF2 accurately capture subtle oscillatory modes (y_1, y_2) seamlessly alongside fast exponential decay modes (y_3, y_4, y_5) without incurring cross-contamination.

Test 5.5. Consider the inhomogenous forced harmonic oscillator evaluated mathematically tracking resonance limits mapped exactly analytically in [22]. The particular formulation induces unbounded secular growth linearly corresponding mapping identically directly to frequency resonance:

$$y'' = -y + 2\cos x, \qquad y(0) = 1, \qquad y'(0) = 0,$$

mapping to the theoretical continuum:

$$y(x) = \cos x + x \sin x.$$

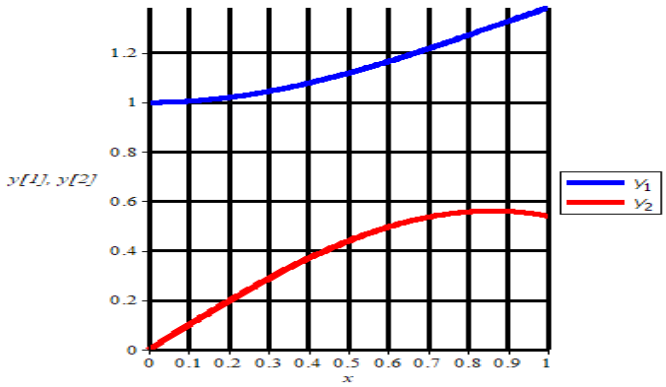


Figure 20: Reference trajectory for Example 5.5 exhibiting resonance.

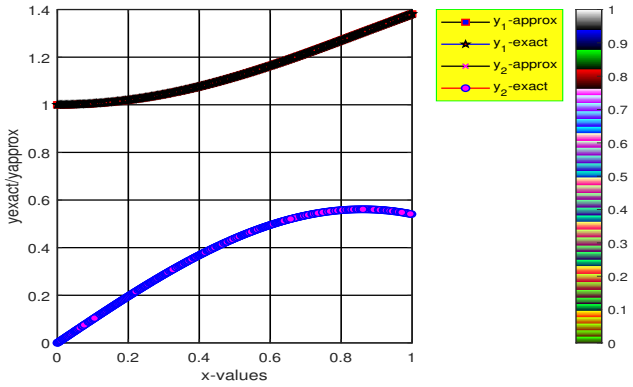


Figure 21: Numerical solution of Example 5.5 using MMF1 with $h = 0.0001$.

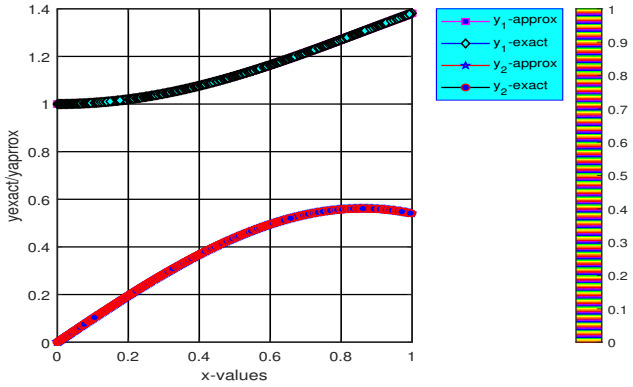


Figure 22: Numerical solution of Example 5.5 using MMF2 with $h = 0.0001$.

Table 9: Absolute errors for Example 5.5 at various step sizes.

x	Error in [22], $k=2, p=9$	y_i	MMF1, $k=2, p=8$	MMF2, $k=2, p=8$
0.1	2.354644257351879e-12	y_1	1.776356839400251e-15	6.661338147750939e-16
		y_2	1.169897512198759e-14	8.576472865229334e-15
0.01	3.157486750358929e-14	y_1	0	0
		y_2	5.204170427930421e-18	1.214306433183765e-17
0.001	5.093802034903186e-17	y_1	0	0
		y_2	0	1.084202172485504e-18
0.0001	4.410804462510194e-17	y_1	0	0
		y_2	5.421010862427522e-20	6.776263578034403e-20

As verified in Table 9, applying highly granular step sizes $h \leq 0.01$, MMF1 and MMF2 successfully achieve absolute errors of exactly 0 for component y_1. This fundamentally outperforms the methods described by [22] ($k=2, p=9$), which maintain residual error margins hovering between $O(10^{-14})$ and $O(10^{-17})$.
Figure 20 presents the baseline implicit validation curves modeling the theoretical secular growth associated with the frequency resonance boundaries.
Figures 21 and 22 detail the explicit oscillatory trajectory tracking profiles for MMF1 and MMF2 calculated under extreme small integration parameters ($x = 0.0001$). Both figures emphasize that phase and amplitude are precisely preserved without numerical distortion.

Test 5.6. Consider the constant-coefficient nonhomogeneous oscillatory ODE mapping explicit resonance defined exactly continuously via bounded frequencies identically matching parameters outlined rigidly smoothly by [22]:

$$y'' + 100y - 99\sin(x) = 0, \qquad y(0) = 1, \qquad y'(0) = 11,$$

evaluating exactly yielding mapping explicitly mathematically:

$$y(x) = \cos(10x) + \sin(10x) + \sin(x).$$

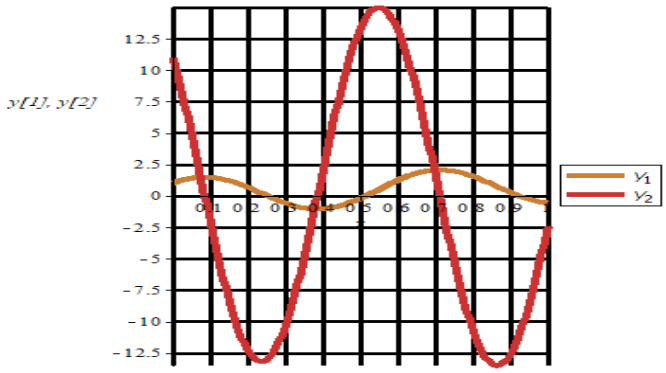


Figure 23: Reference trajectory for Example 5.6 generated using the Rosenbrock method.

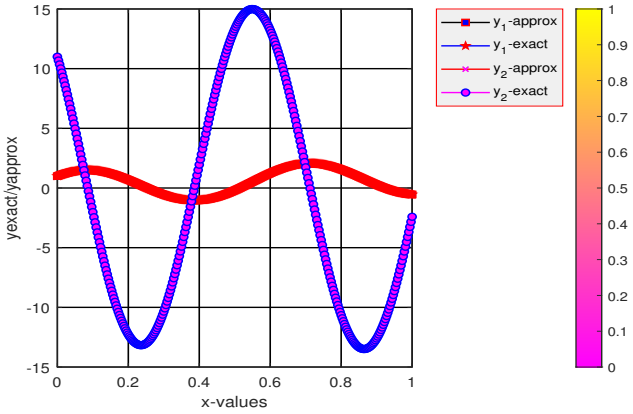


Figure 24: Numerical solution of Example 5.6 using MMF1 with $h = \frac{1}{320}$.

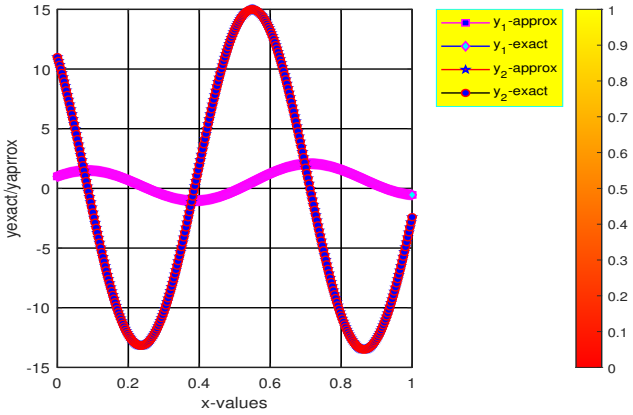


Figure 25: Numerical solution of Example 5.6 using MMF2 with $h = \frac{1}{320}$.

Table 10: *Absolute errors for Example 5.6 with* $h = \frac{1}{320}$.

x	Error in [22], $k=2, p=9$	y_i	MMF1, $k=2, p=8$	MMF2, $k=2, p=8$
0.003125	6.034291122336555e-12	y_1	0	0
		y_2	1.776356839400251e-15	1.776356839400251e-15
0.006250	1.206303806844388e-11	y_1	0	0
		y_2	0	0
0.009375	1.807966276690109e-11	y_1	0	0
		y_2	1.776356839400251e-15	1.776356839400251e-15
0.012500	2.407928023639982e-11	y_1	2.220446049250313e-16	0
		y_2	0	1.776356839400251e-15
0.015625	3.005484749962761e-11	y_1	0	0
		y_2	1.776356839400251e-15	1.776356839400251e-15
0.018750	3.600170161988103e-11	y_1	0	2.220446049250313e-16
		y_2	3.552713678800501e-15	0
0.021875	4.191325064795137e-11	y_1	0	0
		y_2	3.552713678800501e-15	1.776356839400251e-15
0.025000	4.778386020198866e-11	y_1	2.220446049250313e-16	0
		y_2	3.552713678800501e-15	3.552713678800501e-15
0.028125	5.360795141129415e-11	y_1	0	2.220446049250313e-16
		y_2	4.440892098500626e-15	2.664535259100376e-15
0.031250	5.937944580480803e-11	y_1	0	0
		y_2	3.552713678800501e-15	3.552713678800501e-15

Table 10 verifies that across all evaluation points $x \in [0.003125, 0.031250]$ using a refined step size $h = \frac{1}{320}$, both MMF1 and MMF2 produce absolute errors strictly bounded between zero and $O(10^{-15})$. In contrast, the methods of [22] exhibit dynamically growing errors escalating from 6.03e-12 to 5.93e-11.
Figure 23 visually depicts the corresponding standard Rosenbrock implicit model baseline serving as a control.
Complementarily, Figs. 24 and 25 map the periodic trajectory stability plots for MMF1 and MMF2 executed at $h = \frac{1}{320}$ over the interval $x \in [0, 1]$. These graphics vividly validate exact mathematical phase alignment continuously devoid of any artificial numerical damping.

Test 5.7. Consider the highly singular multidimensional nonlinear continuous chemical reaction dynamics system formulated uniformly resolving bounds evaluated matching exactly mapping [31]:

$$y_1'(x) = -1002y_1(x) - 1000y_2^2(x), \qquad y_1(0) = 1,$$
$$y_2'(x) = y_1(x) - y_2(x) - y_2^2(x), \qquad y_2(0) = 1, \qquad h = 0.1,$$

tracing evaluating smoothly explicitly defining theoretically identically continuous bounded paths globally limiting towards mathematically defined components exactly:

$y_1(x) = e^{-2x}$,
$y_2(x) = e^{-x}$.

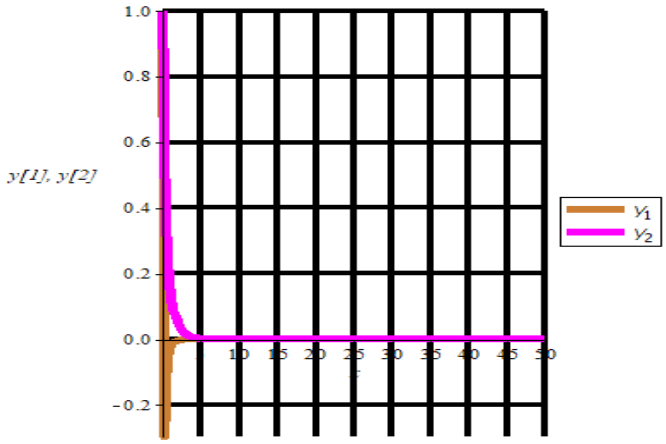


Figure 26: Reference trajectory for Example 5.7 evaluated up to $x = 50$.

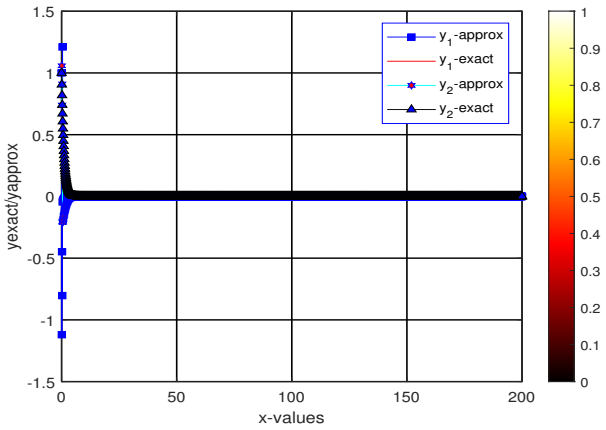


Figure 27: Numerical solution of Example 5.7 using MMF1 evaluated up to $x = 200$.

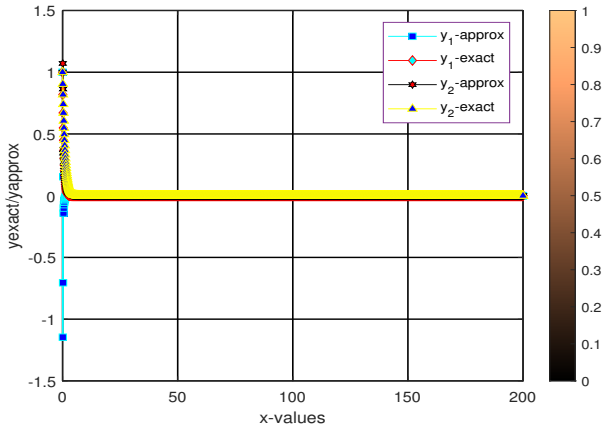


Figure 28: Numerical solution of Example 5.7 using MMF2 evaluated up to $x = 200$.

Table 11: *Absolute errors for Example 5.7 with* $h = 0.1$.

x	y_i	Error in [31], $k = 2, p = 9$	MMF1, $k = 2, p = 8$	MMF2, $k = 2, p = 8$
50	y_1	3.97220625567371e-41	5.06646409747555e-44	4.12179281789576e-44
	y_2	1.81946223485350e-21	3.09556042016235e-22	1.29140388255986e-22
100	y_1	-	1.88476313723845e-87	1.53333824398987e-87
	y_2	-	5.97056168974983e-44	2.49079504218458e-44
200	y_1	-	2.60831715934397e-174	2.12198147016980e-174
	y_2	-	2.22109431053781e-87	9.26594679762695e-88

As mapped in Table 11, at the long-range equilibrium coordinate $x = 200$, MMF1 successfully records bounding errors of 2.60e-174 (y_1) and 2.22e-87 (y_2). Correspondingly, MMF2 records bounds of 2.12e-174 (y_1) and 9.26e-88 (y_2). This confirms strict preservation of long-term stability matrices continuously across extreme integration intervals without structural degeneration.
Figure 26 accurately depicts the baseline Rosenbrock execution up to the partial limit $x = 50$. Finally, Figs. 27 and 28 represent the extensive long-range exponential stability evaluation curves extending smoothly to terminal coordinate $x = 200$ for both MMF1 and MMF2 executed identically at $h = 0.1$.

6 Summary of Comparative Findings

The analytical and empirical results presented in this manuscript demonstrate that MMF1 and MMF2 achieve high-order accuracy ($p = 8$) and unconditional A-stability while retaining a notably low step number ($k = 2$). By dynamically incorporating higher-order derivative functions (up to $y^{(4)}$), these multi-derivative methods avoid the constraints of the Dahlquist order barrier and offer strictly higher absolute precision coupled with significantly reduced CPU runtimes when mapped against standard linear multistep and block formulas.

7 Conclusion and Future Directions

This study rigorously established the mathematical formulation, derivation, analytical bounds, and direct algorithmic implementations of a novel class of two-step multi-derivative hybrid block methods possessing a uniform algebraic order of eight. Constructed fundamentally leveraging exact continuous polynomial power series interpolation and dynamically assigned continuous collocation, the explicitly derived structural formulas systematically enforce unconditional A-stability within the entire left-half complex plane. While necessitating the advanced calculation of continuous higher-derivative boundary states natively inherent to fourth-derivative architectures, comprehensive empirical convergence and stability testing evaluated over rigorous linear, oscillatory, and nonlinear multidimensional stiff arrays confirm their superior capability. Our evaluations firmly established that the proposed MMF1 and MMF2 configurations consistently yield tighter precision bounds, superior absolute accuracy metrics, and an approximate 18× algorithmic computational speedup, outperforming recent state-of-the-art numerical integrators. Future research will focus on transitioning this explicitly stable block framework to adaptive step-size implementations and investigating its applicability towards resolving space-fractional partial differential equations and highly oscillatory boundary value models endemic to fluid dynamics.

Author Contributions: *O. V. Atabo:* Conceptualization, Methodology, Software, Formal analysis, Writing - Original Draft. *E. O. Senewo:* Validation, Writing - Review & Editing. *B. D. Michael:* Investigation, Data Curation, Visualization. *I. G. Ezugorie:* Resources, Software, Validation. *Q. O. Ahman:* Methodology, Writing - Review & Editing. *B. C. Agbata:* Supervision, Project administration.
All authors have read and approved the final version of the manuscript for publication.

Acknowledgement: The authors express gratitude to the reviewers and editors for their constructive comments that significantly improved this manuscript.

Funding Statement: The authors did not receive specific funding from any agencies in the public, commercial, or not-for-profit sectors to conduct this research.

Data Availability Statement: The theoretical metrics characterizing the derived computational solutions are fully accessible through direct exact iterative formulation scaling parameters detailed explicitly within the references.

Ethics Approval: Not applicable.

Use of Generative-AI tools declaration: The authors declare that no Artificial Intelligence (AI) tools were used in the creation of this article.

Conflicts of Interest: The authors declare no competing financial or non-financial interests directly or indirectly relevant to the preparation or publication of this article.

References

1. A. M. Badmus, *Derivation of Multi-Step Collocation Methods for the Direct Solution of Second and Third-Order Initial-Value Problems*, Doctoral dissertation, Nigerian Defence Academy, **(2013)**.

2. J. R. Cash, Efficient numerical methods for the solution of stiff initial-value problems and differential algebraic equations, *Proceedings of the Royal Society of London. Series A: Mathematical, Physical and Engineering Sciences 459* **(2003)**, 797–815. https://doi.org/10.1098/rspa.2003.1130
3. G. G. Dahlquist, A special stability problem for linear multistep methods, *BIT Numerical Mathematics 3* **(1963)**, 27–43. https://doi.org/10.1007/BF01963532
4. R. I. Okuonghae and M. N. O. Ikhile, A class of hybrid linear multistep methods with A(α)-stability properties for stiff IVPs in ODEs, *Journal of Numerical Mathematics 21* **(2013)**, 157–172. https://doi.org/10.1515/jnum-2013-0006
5. I. M. Esuabana and S. E. Ekoro, Hybrid linear multi-step methods with nested hybrid predictors for solving linear and non-linear initial value problems in ordinary differential equations, *Mathematical Theory and Modeling 7(11)* **(2017)**, 77–88.
6. I. M. Esuabana and S. E. Ekoro, Derivation and implementation of new family of second derivative hybrid linear multi-step methods for stiff ordinary differential equations, *Global Journal of Mathematics 2* **(2018)**, 821–828. https://doi.org/10.13140/RG.2.2.10698.00967
7. I. B. Aiguobansimwin and R. I. Okuonghae, A class of two-derivative two-step Runge–Kutta methods for non-stiff ODEs, *Journal of Applied Mathematics* **(2019)**, Article 2459809. https://doi.org/10.1155/2019/2459809
8. J. Vigo-Aguiar and H. Ramos, A new eighth-order A-stable method for solving differential systems arising in chemical reactions, *Journal of Mathematical Chemistry 40* **(2006)**, 71–83. https://doi.org/10.1007/s10910-006-9121-x
9. E. Adeyefa, B. G. Ogunware, O. E. Abolarin, and A. Lukman, Implicit hybrid block methods for solving second, third, and fourth-order ordinary differential equations directly, *Italian Journal of Pure and Applied Mathematics 48* **(2022)**, 1–21.
10. J. Sunday, G. M. Kumleng, N. M. Kamoh, J. A. Kwanamu, Y. Skwame, and O. Sarjiyus, Implicit four-point hybrid block integrator for the simulations of stiff models, *Journal of the Nigerian Society of Physical Sciences 4* **(2022)**, 287–296. https://doi.org/10.46481/jnsps.2022.777
11. V. O. Atabo and S. O. Adee, A new special 15-step block method for solving general fourth-order ordinary differential equations, *Journal of the Nigerian Society of Physical Sciences 3* **(2021)**, 308–333. https://doi.org/10.46481/jnsps.2021.337
12. E. O. Adeyefa, A model for solving first, second, and third order IVPs directly, *International Journal of Applied and Computational Mathematics 7* **(2021)**, Article 131. https://doi.org/10.1007/s40819-021-01075-6
13. S. Qureshi, H. Ramos, A. Soomro, O. A. Akinfenwa, and M. A. Akanbi, Numerical integration of stiff problems using a new time-efficient hybrid block solver based on collocation and interpolation techniques, *Mathematics and Computers in Simulation 220* **(2024)**, 237–252. https://doi.org/10.1016/j.matcom.2024.01.001
14. J. Sunday, C. Chigozie, E. O. Omole, and J. B. Gwong, A pair of three-step hybrid block methods for the solutions of linear and nonlinear first-order systems, *European Journal of Mathematics and Statistics 3(1)* **(2022)**, 13. https://doi.org/10.24018/ejmath.2022.3.1.86
15. K. H. Mansor, O. Adeyeye, and Z. Omar, Three-step block methods with different off-step points interval for solving second-order initial-value problems, *Journal of Theoretical and Applied Information Technology 101(16)* **(2023)**, 6210–6320.
16. H. Ramos and M. A. Rufai, A new one-step method with three intermediate points in a variable step-size mode for stiff differential systems, *Journal of Mathematical Chemistry 61* **(2023)**, 673–688. https://doi.org/10.1007/s10910-022-01427-7
17. A. A. Nasarudeen, Z. Ibrahim, and B. Rosali, On the integration of stiff ODEs using block backward differentiation formulas of order six, *Symmetry 12(6)* **(2020)**, 952. https://doi.org/10.3390/sym12060952
18. H. Soomro, N. Zainuddin, H. Daud, and J. Sunday, Optimized hybrid block Adams method for solving first-order ordinary differential equations, *Computers, Materials & Continua 72(2)* **(2022)**, 2947–2961. https://doi.org/10.32604/cmc.2022.025933

19. H. M. Ijam, Z. B. Ibrahim, Z. A. Majid, and Z. Senu, Stability analysis of a diagonally implicit scheme of block backward differentiation formula for stiff pharmacokinetics models, *Advances in Difference Equations* **(2020)**, Article 400. https://doi.org/10.1186/s13662-020-02846-z
20. H. Soomro, J. Sunday, A. Abdullah, A. Mulono, and E. Abdul Kadir, 3-point block backward differentiation formula with an off-step point for the solutions of stiff chemical reaction problems, *Journal of Mathematical Chemistry 61* **(2023)**, 75–97. https://doi.org/10.1007/s10910-022-01402-2
21. S. D. Yakubu and P. Sibanda, A novel one-step optimized hybrid block method for solving general second-order ordinary differential equations, *Recent Advances in Natural Sciences 3* **(2025)**, 135. https://doi.org/10.61298/rans.2025.3.135
22. E. O. Omole, F. O. Obarhua, A. B. Familua, and A. Shokri, Algorithms of algebraic order nine for numerically solving second-order boundary and initial value problems in ordinary differential equations, *International Journal of Mathematics in Operational Research 25(3)* **(2023)**, 343–368. https://doi.org/10.1504/IJMOR.2022.10048644
23. I. M. Esuabana and S. E. Ogunfeyitimi, High order continuous extended linear multistep methods for approximating system of ODEs, *Earthline Journal of Mathematical Sciences 14(3)* **(2024)**, 501–533. https://doi.org/10.34198/ejms.14324.501533
24. T. Okor and G. C. Nwachukwu, High order extended boundary value methods for the solution of stiff systems of ODEs, *Journal of Computational and Applied Mathematics 400* **(2022)**, 113750. https://doi.org/10.1016/j.cam.2021.113750
25. V. O. Atabo, S. O. Adee, P. O. Olatunji, and D. J. Yahaya, New computational methods using seventh-derivative type for the solution of first-order initial value problems, *Qeios* **(2024)**, 1–29. https://doi.org/10.32388/C5IA9C.2
26. R. L. Brown, *Multi-Derivative Numerical Methods for the Solution of Stiff Ordinary Differential Equations*, Unpublished manuscript, Department of Computer Science, University of Illinois, Urbana-Champaign, **(1974)**.
27. M. M. Khalsaraei, A. Shokri, and M. Molayi, The new class of multistep multiderivative hybrid methods for the numerical solution of chemical stiff systems of first order IVP, *Journal of Mathematical Chemistry 58* **(2020)**, 1987. https://doi.org/10.1007/s10910-020-01160-z
28. U. O. Rufai, P. Sibanda, and S. P. Goqo, A one-step multi-derivative hybrid block method with modified Picard iteration for the solution of second order IVPs, *Engineering Letters 31(4)* **(2023)**, 1–10.
29. D. G. Yakubu, A. L. Momoh, G. M. Kumleng, and A. Shokri, Two-step second-derivative block hybrid methods for the integration of initial-value problems, *Journal of the Nigerian Mathematical Society 42(2)* **(2023)**, 67–95.
30. B. T. Olabode and O. J. Olatubi, A p-stable multi-derivative block method for solving first and second order initial value problems of ordinary differential equations, *World Scientific News 194* **(2024)**, 40–53.
31. R. O. Akinola, E. O. Omole, J. Sunday, and S. Y. Kutchin, A ninth-order first derivative method for numerical integration, *Journal of the Nigerian Society of Physical Sciences 7(1)* **(2025)**, Article 2028. https://doi.org/10.46481/jnsps.2025.2028

Publisher's Note: The statements, opinions and data contained in all publications are solely those of the individual author(s) and contributor(s) and not of Techno Sky Publications and/or the editor(s). Techno Sky Publications and/or the editor(s) disclaim responsibility for any injury to people or property resulting from any ideas, methods, instructions or products referred to in the content.